A pragmatic model for high temperature reactive porous media, with application to ablative materials and biomass pyrolysis

Jean Lachaud
Silicon Valley Initiatives
University of California Santa Cruz
NASA Ames Research Park, Building 19
Moffett Field, CA 94035
USA

jlachaud@ucsc.edu

ABSTRACT

This lecture note presents a generic model for high-temperature reactive porous media. The model is mathematically rigorous but kept as simple as possible to allow simulating complex engineering problems. Detailed heat and mass transport phenomena are modeled. The macroscopic model is obtained by volume averaging over a nonspecific media containing several solid phases and a single gas phase. Only first order terms are kept. The model has been implemented in the Porous material Analysis Toolbox (PATO) available Open source under Software Usage Agreement. As illustration, two applications are presented: ablative heat-shield design and valorization of biomass by pyrolysis.

Contents

Reference: J. Lachaud (2015). A pragmatic model for high temperature reactive porous media, with application to ablative materials and biomass pyrolysis. In: Porous media interaction with high temperature and high speed flows. Eds O. Chazot and F. Panerai. NATO Science and Technology Organization, Paris, France. STO-AVT-261, chapter 9. Under review.

Nomenclature

A_i	Gaseous element/species i
A_j	Arrhenius law pre-exponential factor, SI
c_p	Specific heat, $J \cdot kg^{-1} \cdot K^{-1}$
e	Specific energy, $J \cdot kg^{-1}$
E_j	Arrhenius law activation energy, $J \cdot mol^{-1}$
F	Fractions of solid subphases
h	Specific enthalpy, $J \cdot kg^{-1}$
M	Molar mass, $kg \cdot mol^{-1}$
m_j	Arrhenius law parameter
N_g	Number of gaseous species
n_j	Arrhenius law parameter
p	Pressure, Pa
R	Perfect gas constant, $J \cdot mol^{-1} \cdot K^{-1}$
s	Specific surface, $m^2 \cdot m^{-3}$
y	Element/species mass fractions
ϵ	Volume fraction
μ	Viscosity, $Pa \cdot s$
ω	Production rate, $mol \cdot m^{-3} \cdot s^{-1}$
Π	Pyrolysis gas production rate, $kg \cdot m^{-3} \cdot s^{-1}$
π	Pyrolysis production rate, $kg \cdot m^{-3} \cdot s^{-1}$
ψ	Generic variable
ρ	Density, $kg \cdot m^{-3}$
$\underline{\underline{\beta}}$	Klinkenberg tensor, Pa
θ	Active site density, $mol \cdot m^{-3}$
ζ	Mass stoichoimetric coefficient

χ	Advancement of the pyrolysis reactions
a	Ablative material (gas, fiber, and matrix)
g	Gas phase
p	Solid phase
$\mathcal{F}^*$	Effective diffusion flux, $kg \cdot m^{-2} \cdot s^{-1}$
$\mathcal{Q}^*$	Effective diffusion heat flux, $J \cdot m^{-2} \cdot s^{-1}$
$\underline{\underline{\mathbf{K}}}$	Permeability tensor, s^2
$\underline{\underline{\mathbf{k}}}$	Conductivity tensor, $J \cdot m^{-2} \cdot s^{-1}$
$\mathbf{v}$	Convection velocity, $m \cdot s^{-1}$

1.0 INTRODUCTION

From a material point of view, there are more similarities than differences when studying a space vehicle entering an atmosphere at very high speed and a match burning (Fig. 1). External flow conditions only affect the internal behavior of a porous material through boundary conditions at the interface. The conservation laws within the material are essentially the same and the same mathematical model may be used to analyze their behavior.

a) atmospheric entry of a space vehicle (high-temperature, high-speed flow)

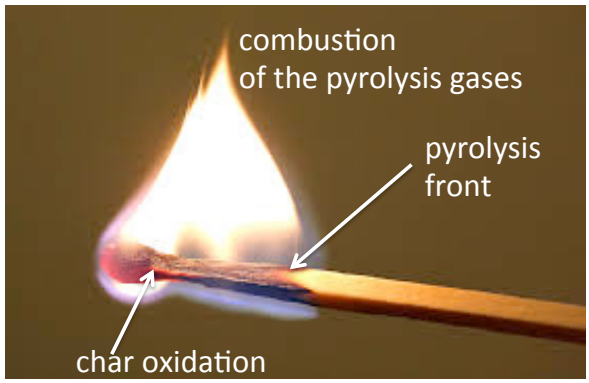

b) match burning

Figure 1: Two high-temperature reactive porous medium applications.

In the literature, we find different type of notations and simplifying hypotheses for different applications. However, the underlying physical phenomena are the same and the mathematical models are mostly equivalent. The objective of this note is to present a generic and pragmatic model, physically complete and mathematically rigorous, but as simple as possible, that can find application in different communities. To cite a few applications, the model presented in this note could be used to model problems as diverse as

- technical engineering solutions: heat shields of space vehicles, rocket nozzle walls, fire protections, car catalytic converters;
- industrial processes: fabrication of carbon-carbon composites by carbon vapor deposition, pyrolysis and gasification of biomass;
- daily uses: a burning match, toasting bread, roasting coffee beans, brewing coffee.

After a detailed description of the model, the model capabilities will be illustrated with the analysis of two applications : ablative heat-shield design and valorization of biomass by pyrolysis.

2.0 MODEL

This section presents a first-order model obtained by volume averaging for decomposing and reacting porous materials, containing several solid/condensed phases and a single gas phase in the continuum regime (low Knudsen number). We wish to provide a general framework, physically complete but mathematically simple and realistic, for engineering analyses and simulations. In most engineering communities dealing with high-temperature reactive porous materials, second-order coupling terms are neglected for practical reasons. Ideally, they would need to be assessed on a case-by-case basis using either direct numerical simulation at the pore scale or well defined elementary experiments. For each application, it is recommended to verify the relevance of the simple model proposed here and assess the possibility of rigorously characterizing and including second-order terms. Practically, if second order terms are hard to determine, it is often because their effect is negligible compared to the propagation of the uncertainties of the main parameters. This can be addressed using sensitivity analyses [1].

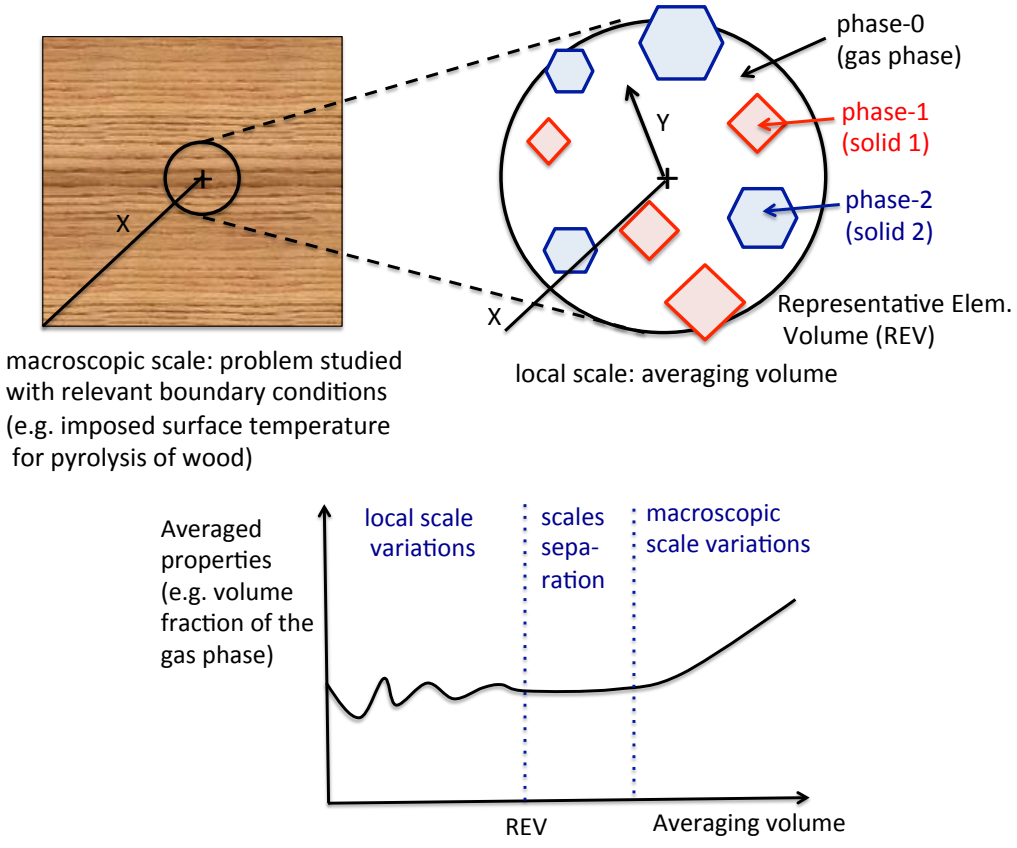

Figure 2: Illustration of the volume averaging approach: a) simplified notation for the tridimensional space coordinates: x: macroscopic scale, y: local scale. b) hypothesis of scale separation.

We will work under the hypothesis of scale separation [2], implying the existence of a representative elementary volume (REV), on which the local variations are smoothed. Using the notations of Fig. 2, the

volume-averaged macroscopic variables are defined as follows

$$< \psi_i(x) >= \frac{1}{REV} \int_{REV} \psi_i(x+y)\, dy \tag{1}$$

where ψ is a physical variable, i is a phase index, x is the macroscopic coordinate, and y is the local coordinate within the REV. The volume fractions, ϵ_i, are computed using the phase indicator γ_i, with $\gamma_i = 1$ within phase i, and $\gamma_i = 0$ outside of phase i such that

$$\epsilon_i =< \epsilon_i(x) >= \frac{1}{REV} \int_{REV} \gamma(x+y)\, dy \tag{2}$$

The volume fractions will be noted ϵ_i to lighten the notations. The intrinsic volume-averaged variables of a given phase i will be noted ψ_i with

$$\psi_i = \psi_i(x) = \frac{< \psi_i(x) >}{\epsilon_i} \tag{3}$$

Using this notation, the total density ρ of a porous material, filled with gas and containing N_p phases, is given by

$$\rho = \epsilon_g\, \rho_g \; + \sum_{i \in [1, N_p]} \epsilon_i \rho_i = \sum_{i \in [0, N_p]} \epsilon_i \rho_i \tag{4}$$

The governing equations for the gasification of the solid/condensed phases, gas and elements/species conservations, momentum conservation, and energy conservation are presented in the following subsections.

2.1 Gasification of the solid/condensed phases

The N_p solid/condensed phases are allowed to loose mass under the effect of heat by pyrolysis, vaporization, and sublimation, and to exchange mass with the surrounding gas through heterogeneous reactions. Each solid phase p_i may decompose following several phenomena and kinetics under the effect of heat (see for example table 1). It is convenient to split each phase i in P_i subphases to model the different degradation mechanisms. The decomposition of subphase j (from solid phase i) produces the elements/species A_k according to the stoichiometric coefficients $\zeta_{i,j,k}$, as follows

$$p_{i,j} \; \rightarrow \sum_{k=1}^{N_g} \zeta_{i,j,k} A_k, \qquad \forall\, i \in N_p,\, \forall\, j \in N_i, \tag{5}$$

where N_g is the total number of gaseous element/species accounted for in the gas mixture. The choice of using elements or species is dictated by the type of chemistry model that is used in the gas phase. It is convenient to use elements for equilibrium chemistry and species for finite-rate chemistry.

The advancement $\chi_{i,j}$ (varying from 0 to 1) of the pyrolysis reactions is modeling using Arrhenius laws of the general form

$$\frac{\partial_t \chi_{i,j}}{(1-\chi_{i,j})^{m_j}} = T^{n_j} \mathcal{A}_j \exp\left(-\frac{E_j}{\mathcal{R}T}\right) \tag{6}$$

The total mass production of species/element k by decomposition of the solid is obtained by summation of the productions of the N_p phases

$$\pi_k = \sum_{i \in [1, N_p]} \sum_{j \in P_i} \zeta_{i,j,k}\, \epsilon_{i,0}\, \rho_{i,0}\, F_{i,j}\, \partial_t \chi_{i,j} \tag{7}$$

where $\epsilon_{i,0}$, $\rho_{i,0}$, and $F_{i,j}$, are respectively the initial (at t=0) volume fraction of phase i, intrinsic density of phase i, and mass fraction of subphase j within phase i.

The overall pyrolysis-gas production is obtained by summing over k and reads

$$\Pi = \sum_{k \in N_g} \pi_k \tag{8}$$

To model heterogenous chemistry, the effective volume-averaged mass-fraction of a reacting solid phase i may be conveniently modeled as [3]

$$y_i = \frac{s_i \, \theta_i}{\epsilon_g} \tag{9}$$

where s_i is its specific surface and θ_i its active site density. This allows introducing the solid phases in the homogeneous chemistry mechanism, to solve homogeneous and heterogeneous finite-rate chemistry in a coupled manner, and compute with improved accuracy and numerical stability the heterogeneous reaction rates ω_k^i.

The average mass evolution for each solid phase is obtained by summing over all contributions

$$\partial_t(\epsilon_i \rho_i) = \sum_{j \in P_i} \epsilon_{i,0} \rho_{i,0} F_{i,j} \partial_t \chi_{ij} + \sum_{k \in N_g} \omega_k^i M_k \tag{10}$$

Possible structural changes (separately affecting ϵ_i and ρ_i) depend on the type of phenomena and materials involved and need to be assessed on a case-by-case basis. Also, terms accounting for shrinkage or swelling (due to temperature variations, for example) may be added. In this latter case, solid flux divergence terms need to be added in the conservation equations to conserve mass and energy.

2.2 Mass conservation: gas, species/elements

The gaseous mass conservation equation includes a production term (right-hand side) to account for the total gas production by the solid, noted Π, and reads

$$\partial_t(\epsilon_g \rho_g) + \partial_{\mathbf{x}} \cdot (\epsilon_g \rho_g \mathbf{v_g}) = \Pi \tag{11}$$

The conservation equations for the N_g element/species mass fractions are included to accurately model element/species transport and chemistry within the pores of the material. The conservation equations for the element/species mass fractions (y_k) read [4]

$$\partial_t(\epsilon_g \rho_g y_k) + \partial_{\mathbf{x}} \cdot (\epsilon_g \rho_g y_k \mathbf{v_g}) + \partial_{\mathbf{x}} \cdot \mathcal{F^*}_k = \pi_k + \epsilon_g \omega_k M_k, \; \forall \, k \in N_g. \tag{12}$$

Here, as explained earlier, we neglect second-order coupling terms (e.g. the local dispersion from the diffusion/convection coupling [2]). In the case of finite-rate chemistry, the chemistry production terms ω_k are obtained by resolution of a chemistry mechanism. In the case of equilibrium chemistry, these terms are null, and the gas composition is directly computed from the local elemental composition, temperature, and pressure. $\mathcal{F^*}_k$ is the effective diffusion flux of the k^{th} element/species (developed in section 3).

2.3 Momentum conservation

The average gas velocity is obtained by resolution of the momentum-conservation equation. In porous media, the volume-averaged momentum conservation may be written as [2]

$$\mathbf{v_g} = -\frac{1}{\epsilon_g}\left(\frac{1}{\mu}\underline{\underline{\mathbf{K}}} + \frac{1}{p}\underline{\underline{\beta}}\right)\cdot\partial_{\mathbf{x}}p \tag{13}$$

Most of the materials are anisotropic, therefore, the permeability - $\underline{\underline{\mathbf{K}}}$ - is a second order tensor. The contribution $\underline{\underline{\beta}}$ is the Klinkenberg correction to account for slip effects (at the pore scale) when the Knudsen number (ratio of the mean free path to the mean pore diameter) is not very small. The Forchheimer correction may also be used to account for passability in the case of high velocity effects at the pore scale (flow separation in the continuum regime).

2.4 Energy conservation

Under the thermal equilibrium assumption, the energy conservation may be written as

$$\partial_t(\rho_a e_a) + \partial_{\mathbf{x}}\cdot(\epsilon_g\rho_g h_g\mathbf{v_g}) + \partial_{\mathbf{x}}\cdot\sum_{k=1}^{N_g}(\mathcal{Q}^*{}_k) = \partial_{\mathbf{x}}\cdot(\underline{\underline{\mathbf{k}}}\cdot\partial_{\mathbf{x}}T) + \mu\epsilon_g^2(\underline{\underline{\mathbf{K}}}^{-1}\cdot\mathbf{v_g})\cdot\mathbf{v_g} \tag{14}$$

where the total (storage) energy of the porous medium is the sum of the energy of its phases

$$\rho_a e_a = \epsilon_g\rho_g e_g + \sum_{i\in[1,N_p]}\epsilon_i\rho_i h_i \tag{15}$$

The second and third terms of the left-hand side are the energy convected (advection) and the energy transported by effective diffusion of the gases (developed in section 3), respectively. The second term on the right-hand side is the energy dissipated by viscous effects in the Darcian regime [5]. It is very small and can be neglected. Heat transfer is conveniently modeled as an effective diffusive transfer (Fourier's law). The effective conductivity - $\underline{\underline{\mathbf{k}}}$ - is a second order tensor accounting for conduction in the solid, conduction in the gas, radiative heat transfer, including possible coupling terms between these heat transfer modes and deviation by coupling with other terms. On a case-by-case basis, more advanced and accurate models can be derived and data for them obtained. According to Puiroux et al. [6], solid and gas phases are in thermal equilibrium as long as the Peclet number for diffusion of heat within the pores is small ($Pe = \epsilon_g\rho_g c_{p,g} d_p v_g/k_g$). It is important to mention that strong enthalpy changes in the solid phases may also lead to thermal non-equilibrium, this time between the solid phases themselves.

Effective conductivity is generally the main mode of heat transport. To solve implicitly Eq. 14, it is therefore convenient to develop it and express it in terms of temperature. The first term reads

$$\partial_t(\rho_a e_a) = \partial_t(\epsilon_g\rho_g e_g) + \sum_{i\in[1,N_p]}\partial_t(\epsilon_i\rho_i h_i) \tag{16}$$

$$= \partial_t(\epsilon_g\rho_g(h_g - p/\rho_g)) + \sum_{i\in[1,N_p]}[\epsilon_i\rho_i c_{p,i}\partial_t T + h_i\partial_t(\epsilon_i\rho_i)] \tag{17}$$

Eq. 14 can then be rearranged as follows

$$\sum_{i\in[1,N_p]}\left[\left(\epsilon_i\rho_i c_{p,i}\right)\partial_t T\right]-\partial_{\mathbf{x}}\cdot(\underline{\underline{\mathbf{k}}}\cdot\partial_{\mathbf{x}}T)=\left|\begin{array}{l}-\sum_{i\in[1,N_p]}h_i\partial_t(\epsilon_i\rho_i)\\-\partial_t(\epsilon_g\rho_g h_g-\epsilon_g p)+\partial_{\mathbf{x}}\cdot(\epsilon_g\rho_g h_g\mathbf{v_g})\\+\partial_{\mathbf{x}}\cdot\sum_{k\in N_g}(\mathcal{Q}^*{}_k)+\mu\epsilon_g^2(\underline{\underline{\mathbf{K}}}^{-1}\cdot\mathbf{v_g})\cdot\mathbf{v_g}\end{array}\right. \tag{18}$$

and implicitly solved in temperature, possibly lagging the right-hand side terms.

3.0 APPLICATIONS

In this section, two applications are presented: ablative heat-shield design and valorization of biomass by pyrolysis. Despite the obvious differences in material properties and environmental conditions, the same generic model presented above may be used for these applications. The generic model is implemented in the Porous Material Analysis Toolbox (PATO) [7, 8]. PATO is used for the simulations presented in this section.

3.1 Ablative heat-shield design

Space exploration missions often include entering a planet atmosphere at hypersonic speed. A high enthalpy hypersonic shock forms around the spacecraft and kinetic energy is progressively dissipated into heat [9]. Heat is transferred to the surface of the spacecraft by radiation and convection. A suitable heat shield is needed to protect the payload. The level of heat flux increases with entry speed and atmosphere density. For moderate speed entry, typically below $7.5\,km/s$, and mild heat fluxes, up to $1\,MW/m^2$, reusable materials are an adequate solution. A famed example is the ceramic tile used on the Space Shuttle Orbiter. For entry speeds higher than $8km/s$, heat fluxes exceeding $1.5\,MW/m^2$, and entry into high-density atmospheres requires the use of ablative materials for Thermal Protection Systems (TPS). These mitigate the incoming heat through phase changes, chemical reactions, and material removal [10].

A critical problem in the design of ablative TPS is the choice of a heat shield material and its associated material response model. In the past, dense carbon/carbon and carbon/resin composites have been widely used for many ablative applications [10, 11], including space exploration [12]. The last decade has seen a renewed effort by scientists and engineers toward the development of a new class of carbon/phenolic (C/P) ablators specifically designed for high altitude braking in Earth and Mars atmospheres. This new class of C/P composites is made of a carbon fiber preform partially impregnated with a low-density phenolic resin (Figure 3). They are very light with an overall density around $200kg/m^3$, are good insulators, and display sufficient mechanical properties for atmospheric reentry. A successful example is the phenolic-impregnated carbon ablator (PICA) developed at the NASA Ames Research Center [13] and flight qualified during the recent reentry missions of Stardust (Earth reentry at $12.7\,km/s$) [14] and the Mars Science Laboratory (Mars entry at $5.5\,km/s$) [15, 16]. This innovative development has been followed by the Space Exploration Technologies Corp. (SpaceX) with PICA-X , used on the commercial Dragon capsule,[1] and by Airbus Defense and Space with ASTERM, selected by the European Space Agency for future missions [17].

During atmospheric entry, low-density carbon/phenolic ablative materials undergo thermal degradation and ultimately recession captured by the following physico-chemical phenomena (Figure 3):

- Solid Pyrolysis (pyrolysis zone). Zone where the phenolic polymer thermally decomposes and progressively carbonizes into a low density carbon form, losing mass while releasing pyrolysis gases - hydrogen and phenol are shown as examples in Figure 3. Detailed gas composition is available in the literature [18].

- Pyrolysis-gas Transport and Chemistry (char layer = coking zone and ablation zone). Zone where the pyrolysis gases released by solid pyrolysis percolate and diffuse to the surface through the network of pores. Reactions within the pyrolysis-gas mixture (homogeneous reactions) and between pyrolysis gases and the char take place with possible coking effects (heterogeneous reactions). Mixing and reaction of the pyrolysis gases with boundary layer gases into the pores of the material occur when boundary layer gases penetrate in the material by forced convection or due to fast diffusion at low pressures.

[1] http://www.spacex.com/news/2013/04/04/pica-heat-shield, retrieve Jan 1, 2014.

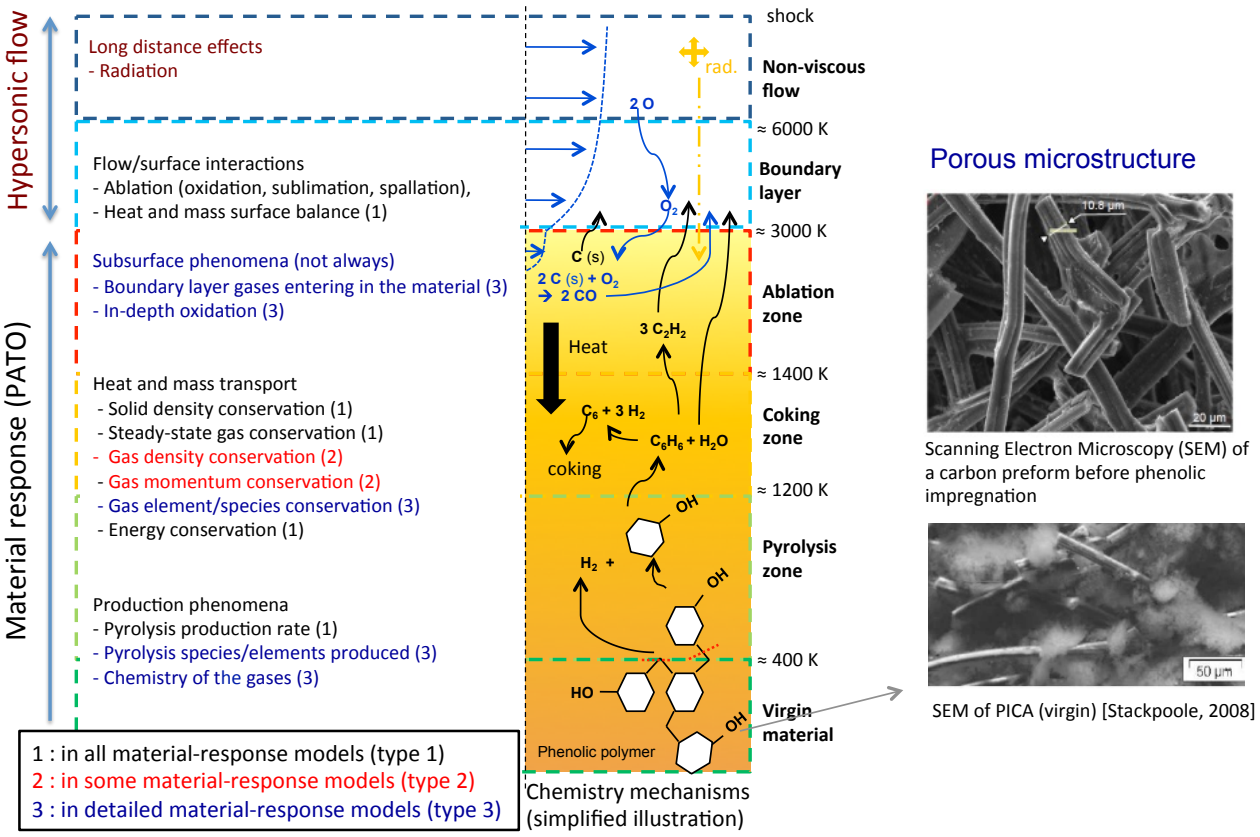

Figure 3: Phenomenology of porous carbon/phenolic ablative materials

- Ablation Chemistry (ablation zone). Zone where after charring (and possible coking), the material is removed by ablation and the outer surface recedes. Depending on entry conditions, ablation may be caused by heterogeneous chemical reactions (oxidation, nitridation), phase change (sublimation), and possibly mechanical erosion (often called spallation).

A review of the open literature has revealed three levels of models used in twenty-five numerical simulation tools [19]. The first level (1), based on the state-of-the-art Charring Material Ablation [20] model, initially developed for the dense ablators in the 1960s, is implemented in all design codes. The core phenomena of the pyrolysis/ablation problem are modeled but many simplifications are used. A major simplification is that the momentum-conservation is not implemented, meaning that the direction of the pyrolysis gas flow and the internal pressure need to be arbitrarily prescribed by the user. This type (1) model is well adapted for unidimensional, quasi steady-state, and equilibrium chemistry conditions with constant element fractions. Type (1) models [20–22] have enabled successful porous heat-shield design but have required the use of large safety margins to compensate for possible prediction errors [15]. However, post flight analyses of MSL flight data have shown that type (1) material models provide slightly inaccurate flight predictions when using ground data [16]. The second level (2) of modeling includes the implementation of the momentum conservation. This ca-

j	Pyrolysis of phenolic matrix	Peak (K)	$F_{2,j}$	$A_{2,j}$	$E_{2,j}$	$m_{2,j}$	$n_{2,j}$
	Model (Sykes76/Goldstein69/Trick97)	S./T.	S.	G.	G.	G.	G.
1	$p_{2,1} \rightarrow H_2O\,(physisorbed)$	373	0.01	$8.56 \cdot 10^3$	$7.12 \cdot 10^4$	3	0
2	$p_{2,2} \rightarrow 0.69\,H_2O + 0.01 C_6H_6$ $+0.01 C_7H_8 + 0.23 C_6H_6O$	773	0.24	$8.56 \cdot 10^3$	$7.12 \cdot 10^4$	3	0
3	$p_{2,3} \rightarrow 0.09\,CO_2 + 0.33\,CO + 0.58\,CH_4$	873	0.03	$4.98 \cdot 10^8$	$1.70 \cdot 10^5$	3	0
4	$p_{2,4} \rightarrow H_2$	1073	0.06	$4.98 \cdot 10^8$	$1.70 \cdot 10^5$	3	0

Table 1: Pyrolysis balance equations and kinetic parameters.

pability is found in a few design codes and in several recent analysis codes allowing the determination of gas flow directions for constant element/species mixtures. The model presented in this lecture note is typically a Type (3) model. It includes element or species conservation equations, and associated equilibrium or finite-rate chemistry models, for a more rigorous modeling of heat and mass transport phenomena. One interesting feature of the type (3) generic model is that it can reproduce the results of the simplified approaches, when used with the same simplifications.

We propose here a simple uni-dimensional illustration. We use as a support the community-defined ablation test-case 1.0 [23] and compare type 1, type 2, and type 3 code results, simply using the generic model with different levels of simplification. The material of the case is the Theoretical Ablative Composite for Open Testing (TACOT), which is a low-density carbon/phenolic ablator. In volume, TACOT is made of 10% of carbon fibers (phase-1), 10% of phenolic resin (phase-2), and is 80% porous (phase-0: gas). Therefore its composition and properties are comparable to NASA's Phenolic Impregnated Carbon Ablator [13, 21]. The properties of TACOT are open and available upon request. As shown in figure 4, a sample of TACOT of 5 cm is heated on one side at 1644K for 1 minute at atmospheric pressure and cooled down by re-radiation for 1 minute. Adiabatic boundary conditions are used at the bottom. The initial conditions are: p= 1atm (101325 Pa), T= 300K, sample length: 0.05 m. The initial gas composition in the material is left open. We use pyrolysis gases at equilibrium for the type 2 model because this is the usual practice. We use dry air for the finite-rate chemistry case because it makes more sense. The type 2 model used is the one presented in the ablation test-case document and in the TACOT definition file [23]. We believe that the finite-rate chemistry models initially proposed in the TACOT definition file can be significantly improved. Therefore, we use here what we think is a better set of data. The high-fidelity pyrolysis model provided in table 1 and derived from literature data is used.

A reduced 22-species homogeneous finite-rate chemistry mechanism derived from the combustion database of Blanquart [24] is temporarily used to model the finite-rate chemistry of the pyrolysis gases. The list of species is shown in figure 7. We do not provide the complete mechanism as it lacks validation in the context of ablative materials. It is still used here because there is no other well founded mechanism available in the literature for our application. The first graph (figure 5) shows the excellent agreement between PATO used as type 2 and FIAT (type 1), showing that in this simple configuration type 1 and type 2 codes provide similar results. Figure 6 shows a comparison of the thermal response when using finite-rate chemistry versus equilibrium chemistry. The difference is explained by the fact that the pyrolysis gas enthalpies are significantly different (equilibrium vs. finite-rate). Figure 7 shows the evolution of the non-equilibrium pyrolysis gas composition as it is convected through the material towards the surface - in the absence of diffusion here. It is obvious that in this case the finite-rate chemistry model used in the material will have a strong influence on the predicted species in the boundary layer and that the equilibrium assumption would not be correct. It is interesting to note that a large amount of benzene (A1) is injected in the boundary layer according to the finite-rate chemistry model used whereas benzene is not even present when using equilibrium chemistry. Following this study enabled by the

generic model, detailed experiments are being carried out in the ablation community to develop and validate finite-rate chemistry mechanisms for this new class of materials [25].

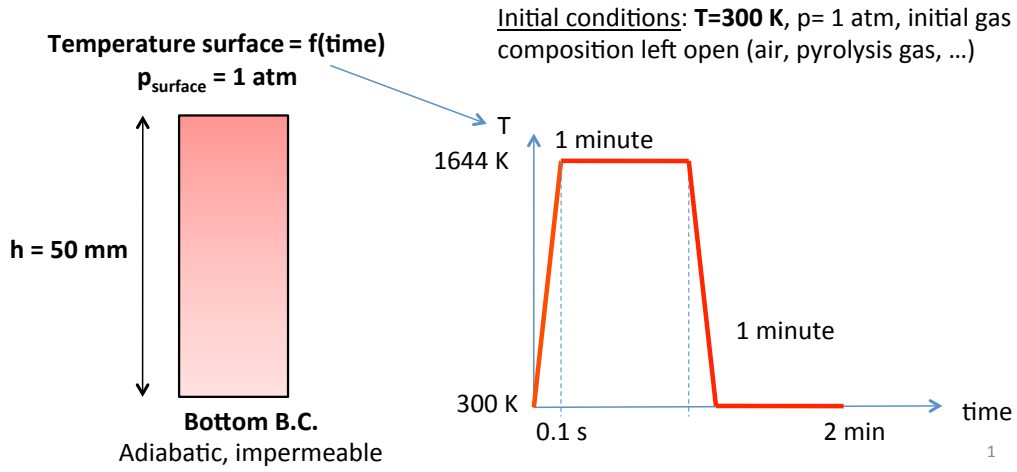

Figure 4: Schematic description of test-case 1.0

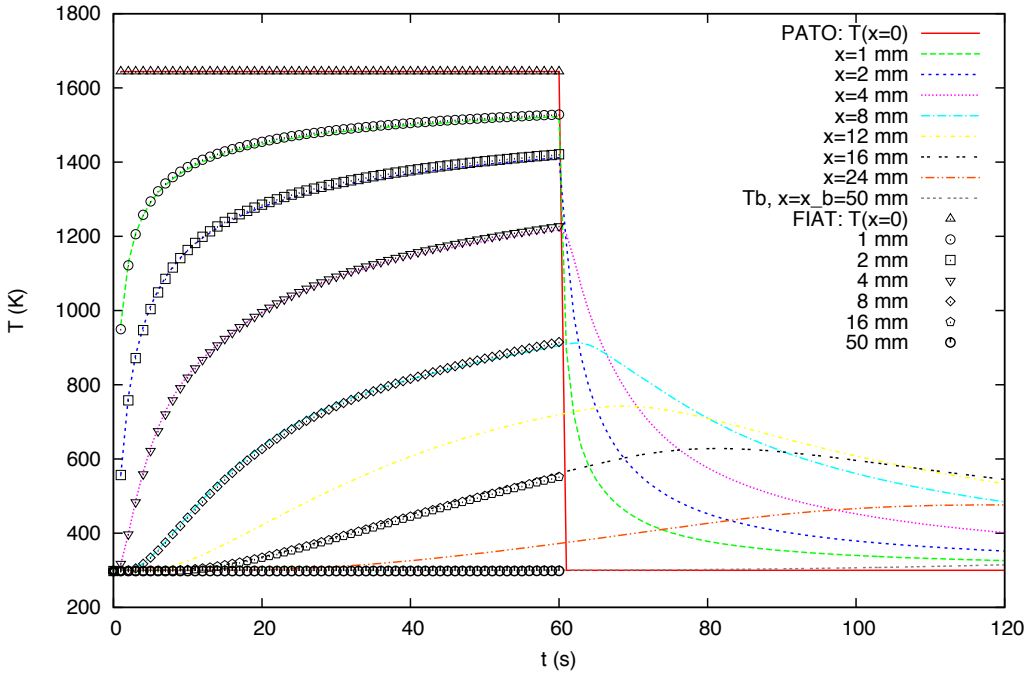

Figure 5: Test-case 1.0: comparison of thermal response between PATO-type2 and FIAT (type1)

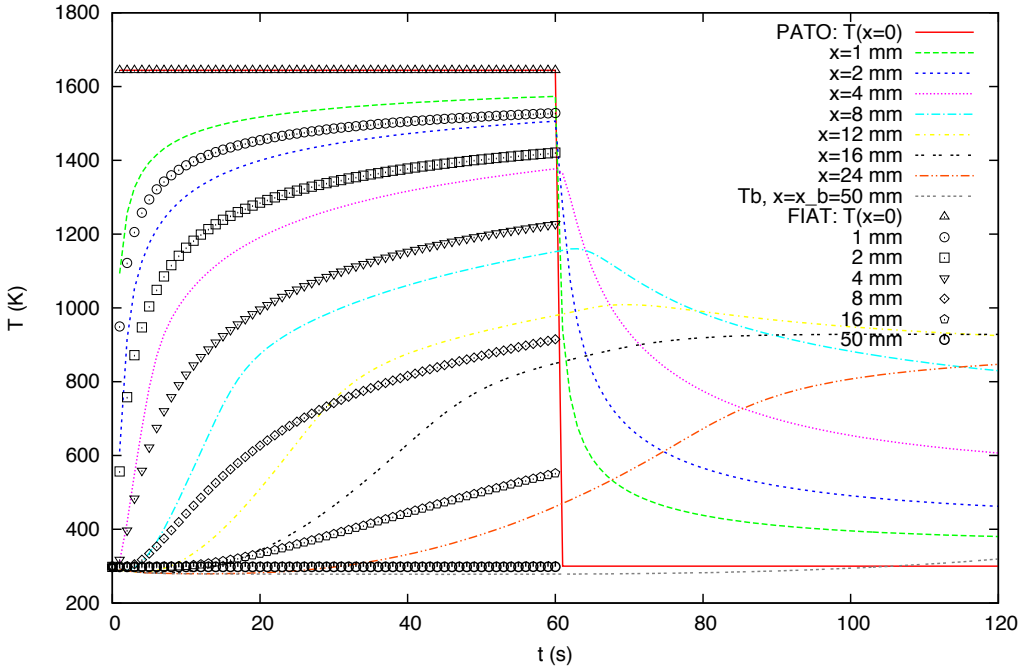

Figure 6: Test-case 1.0: comparison of thermal response between PATO-type3 and FIAT (type 1)

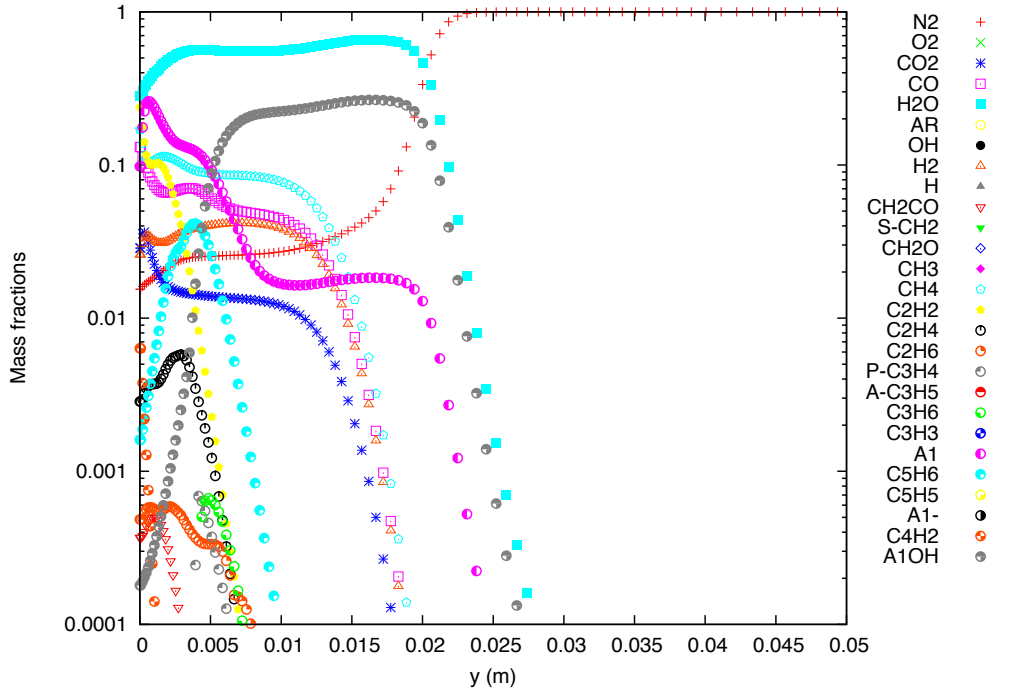

Figure 7: Test-case 1.0 at 60 seconds: PATO-type3 - Blanquart 22 species - diffusion neglected [7]

3.2 Pyrolysis of lignocellulosic biomass

Pyrolysis is one of the many thermochemical processes available to reduce biomass wastes and/or transform biomass in added value products [26]. This process has been widely studied in the past [27]. With the climate change concerns, there is currently a renewed interest for this topic, especially for the pyrolysis of lignocellulosic biomass, with wood as the main representative [28].

There are two types of wood, namely hard wood and soft wood. Softwood consists mainly of long (3 to 5 mm) cells called tracheids which are about 20 to 80 μm in diameter. Hard wood can me modeled as an assembly of cells (wood fibers) to which nutrients and water are brought through vessels. The micrographs of pyrolyzed Niaouli wood (Melaleuca quinquenervia) from Fig. 8 clearly reveal this hard wood structure. Wood fibers are elongated quasi-cylindrical cells; their length is of the order of several millimeters, and their diameter is of the order of 10 μm. From a pyrolysis modeling perspective, the content of the cells can be considered to be water. The walls are made of lignocellulose.

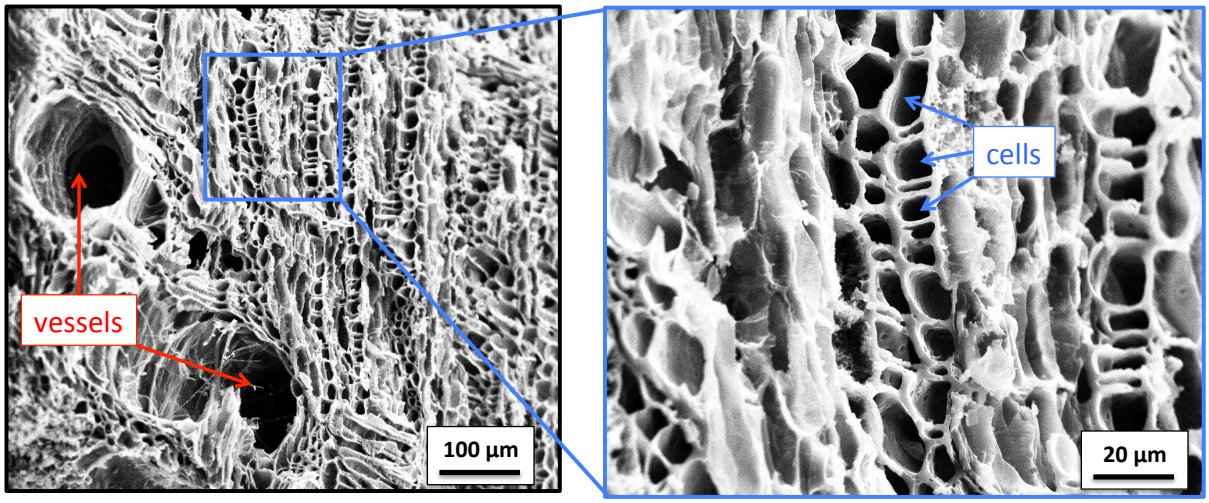

Figure 8: Scanning electron micrographs of Niaouli wood (Melaleuca quinquenervia), pyrolyzed at 500°C for 15 minutes, showing empty cells and vessels (University of New Caledonia).

As represented in Fig. 9, the core component of lignocellulose is cellulose, a β(1-4)-linked chain of glucose molecules. Hydrogen bonds between different layers of the polysaccharides contribute to the resistance of crystalline cellulose to degradation. Hemicellulose is composed of various 5-and 6-carbon sugars such as arabinose, galactose, glucose, mannose and xylose. Lignin is composed of three major phenolic components, namely p-coumaryl alcohol (H), coniferyl alcohol (G) and sinapyl alcohol (S). Lignin is synthesized by polymerization of these components and their ratio within the polymer varies between different plants, wood tissues and cell wall layers. Cellulose, hemicellulose and lignin form structures called microfibrils, which are organized into macrofibrils that mediate structural stability in the plant cell wall [29].

Most pyrolysis studies focus on modeling a chip of wood, non differentiating hard and soft woods and using macroscopic experimental data to model the overall heat transfer and pyrolysis processes. As for ablation, we find different levels of modeling in the literature, not yet categorized but that could fell under the same type 1, type 2, and type 3 nomenclature, as represented in Fig. 10. Under the effect of heat in the absence of oxygen, wood is first desiccated (10 to 50% of its initial mass is water). Then it is pyrolyzed. Pyrolysis products are chiefly methane, carbon monoxide and dioxide, hydrogen, condensable gases (like phenol), and tar. The residue

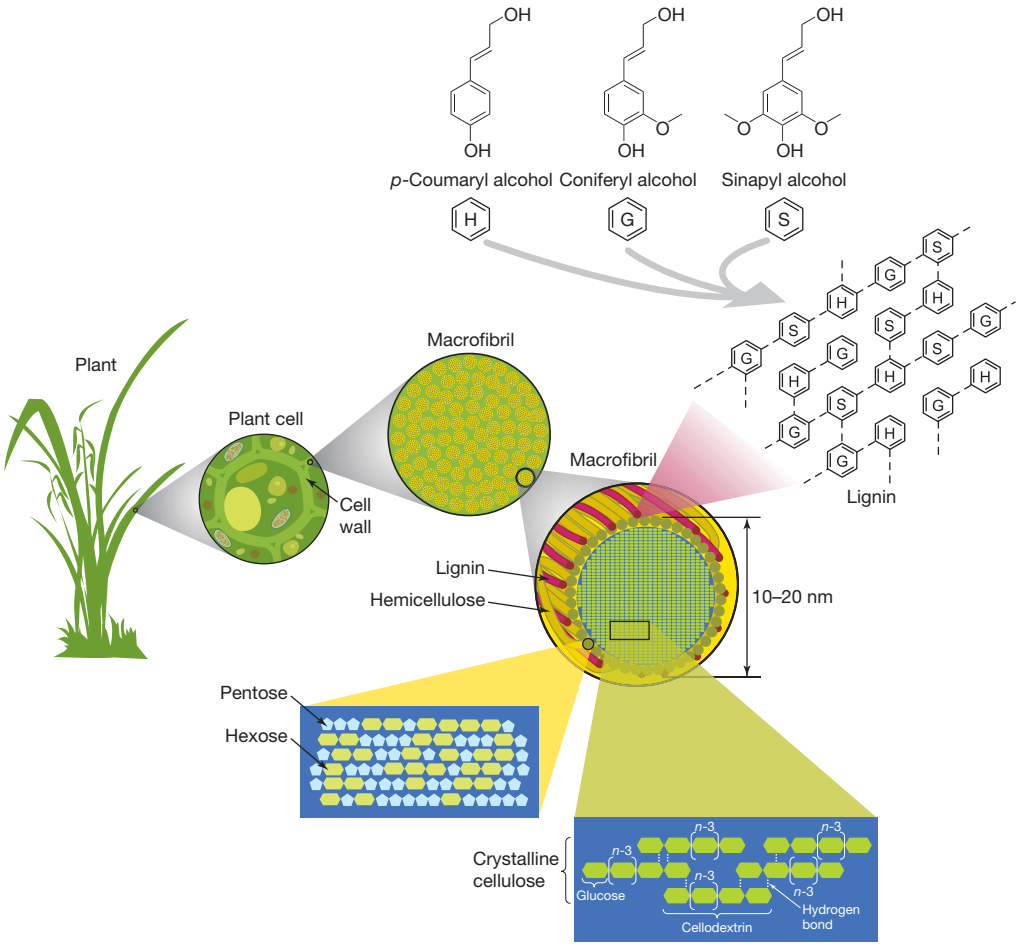

Figure 9: Representation of the multiscale structure of ligno-cellulosic biomass. Schematic adapted from [29] by [30] with authorization from Nature (open access).

is an almost pure carbon char, storing mineral matter (found under the form of ashes after combustion).

The most advanced drying/pyrolysis models consider wood as a N_p condensed/solid phase porous medium. The most detailed mechanism available in the literature models the 3 solid phases of lignocellulose, obtained from a compilation of literature data on cellulose, hemicellulose, and lignin decomposition mechanisms [31]. Adsorbed water is sometimes considered as a fourth phase [28]. One added difficulty is to obtain reliable thermochemical data for the wood species studied. Experimentally, effective properties are obtained in virgin and char states. Linear interpolation is used between these two states. Decomposing wood data are estimated by interpolation between virgin and char state measured values [28].

We present below a simulation of Niaouli pyrolysis using the generic model of section 2. From similar species, we estimated the solid mass fractions to be 37% of cellulose, 20% of hemicellulose, and 43% of lignin. A humidity ratio of 20% has been accounted for under the form of adsorbed water. As a first approximation we used beech wood thermochemical properties [28], because data on Niaouli are not yet available. In this simulation, we used the equilibrium chemistry assumption, and elemental pyrolysis gas mass fractions of C: 0.236, H: 0.413, O: 0.301, N: 0.05. We used the geometry and boundary conditions of the ablation test-case 1.0

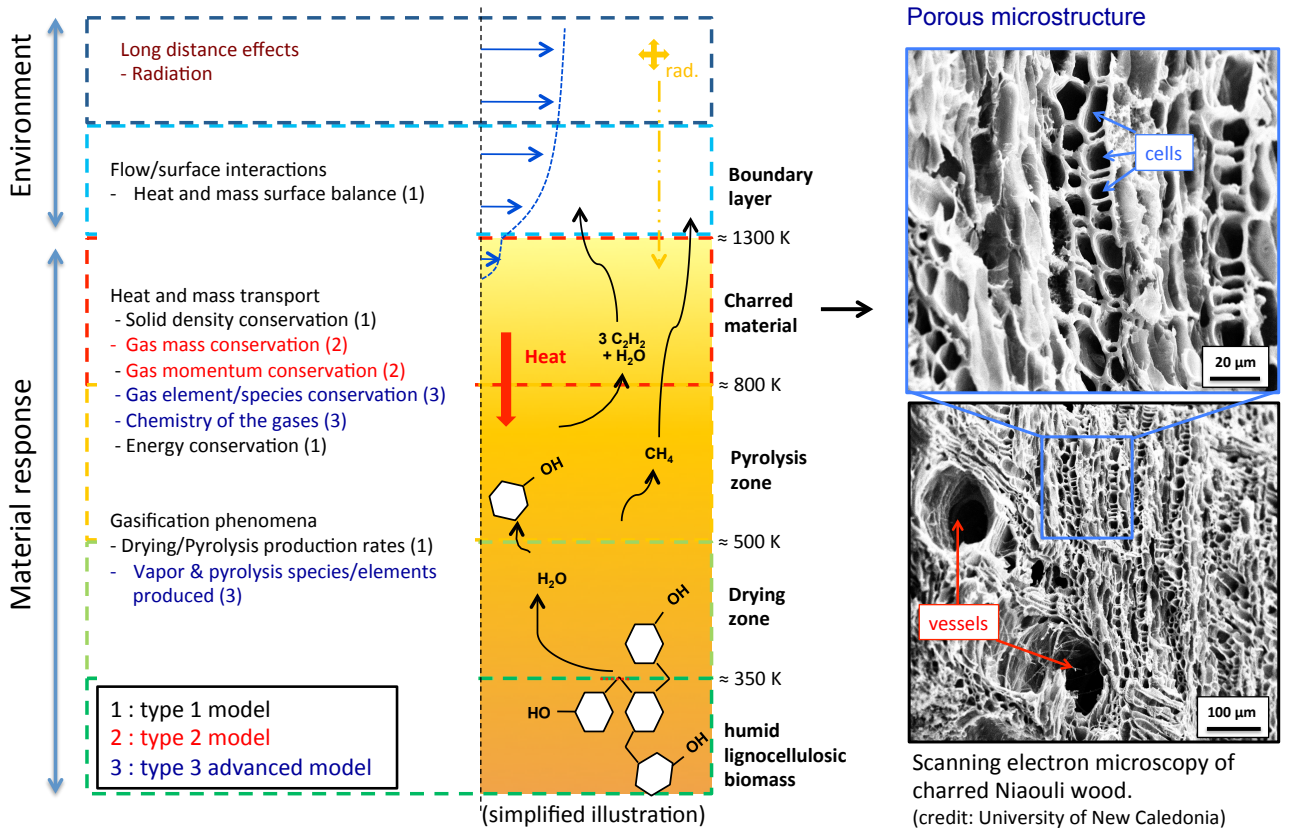

Figure 10: Phenomenology of wood pyrolysis

presented in the previous subsection, with a surface temperature of 900 K kept at the plateau for 8 minutes. The results are represented on Fig. 11; several steps are observed, corresponding to water vaporization, pyrolysis of hemicellulose, pyrolysis of cellulose, and finally pyrolysis of lignin. We see that according to the simulation it takes about 6 minutes to fully pyrolyse the wood chip. This is in qualitative agreement with preliminary experiments carried out at the university of New Caledonia.

Depending on the heating rate, temperature, pressure, and ratio of cellulose-hemicellulose-lignin, one may produce different qualities and ratios of char/gas/oil. This is an appealing challenge for the sustainable energy community but it is hard to model due to the lack of quantitative experimental data [32]. Detailed experimental characterizations of the properties of the materials, of the nature of the gases produced by pyrolysis, added to an analysis of the heterogeneous and homogeneous chemistry occurring within the pores, will be needed in order to predict with some degree of accuracy the nature of the gases and bio-oils produced and help optimize industrial processes. To help in this direction, the generic model can be used to extract relevant data from elementary experiments as well as contribute to the understanding of overall physical phenomena and couplings.

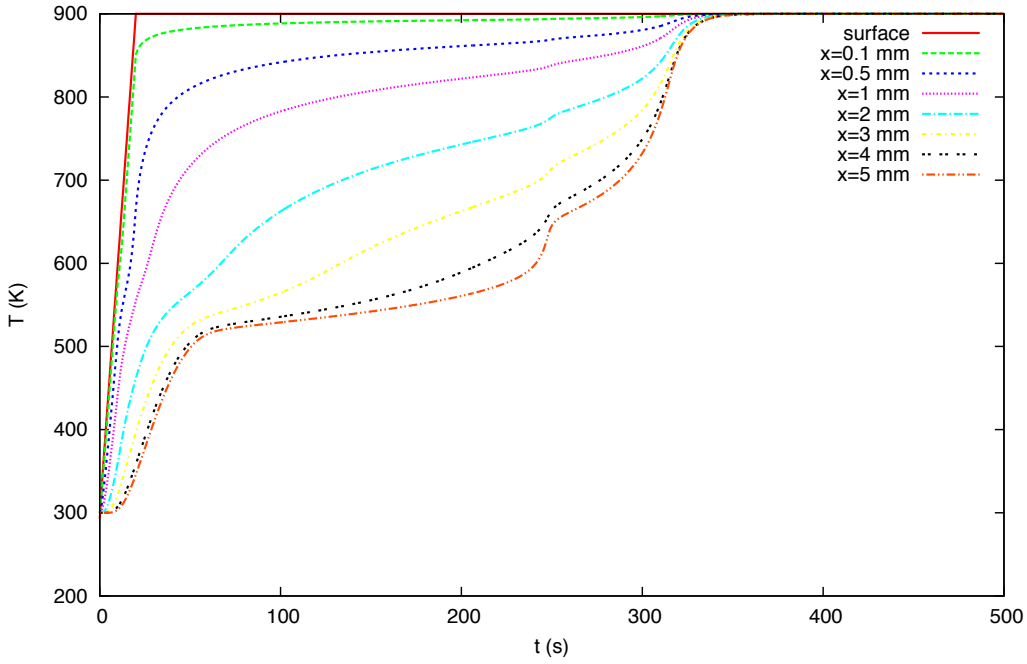

Figure 11: Simulation of the pyrolysis of a 10 mm Niaouli wood chip at 900 K

4.0 CONCLUSION

This note presents a first-order model obtained by volume averaging for decomposing and reacting porous materials, containing several solid/condensed phases and a single gas phase in the continuum regime (low Knudsen number). It provides a general framework, physically complete but mathematically simple and realistic, for engineering analyses and simulations. Two applications are presented as illustrations : ablative heat-shield design and pyrolysis of lignocellulosic biomass. The simulation tool used for the illustrations is distributed Open Source by the NASA Ames Research Center under Software Usage Agreement. Please contact the author for more information.

ACKNOWLEDGMENTS

The presented research on ablative materials is supported by the NASA Space Technology Research Grants Program (grant NNX12AG47A). I would like to thank N. Selmaoui-Folcher, director of the PPME laboratory (University of New Caledonia), for hosting me as an associate researcher and F. Anstett as an intern, to conduct research on biomass pyrolysis. Biomass research is supported by the start-up *C la Vie* (Noumea, New Caledonia) and the French Ministry for Research (innovative start-up emergence grant "iLab" for the project *Carbon Pacific*). Contributions from G. L. Vignoles (University of Bordeaux, France), F. Panerai and N. N. Mansour (Nasa Ames Research Center, California), T. E. Magin, J. B. Scoggins and V. Leroy (von Karman Institute for Fluid Dynamics, Belgium), and M. Meyer and F. Anstett (University of New Caledonia), are gratefully acknowledged.

REFERENCES

[1] Tang, K., Congedo, P., and Abgral, R., "Sensitivity analysis using anchored ANOVA expansion and high order moments computation." *International Journal for Numerical Methods in Engineering*, Vol. available online, 2015, DOI : 10.1002/nme.4856.

[2] Whitaker, S., *The method of volume averaging*, Kluwer Academic Publisher, Dordrecht, The Netherlands, 1999.

[3] Lachaud, J., Cozmuta, I., and Mansour, N. N., "Multiscale Approach to Ablation Modeling of Phenolic Impregnated Carbon Ablators," *Journal of Spacecraft and Rockets*, Vol. 47, No. 6, 2010, pp. 910–921, doi: 10.2514/1.42681.

[4] Giovangigli, V., *Multicomponent flow modeling*, Birkhuser, Boston, 1999.

[5] Ene, H. J. and Sanchez-Palencia, E., "On Thermal Equation for Flow in Porous Media," *International Journal of Engineering Science*, Vol. 20, No. 5, 1982, pp. 623–630.

[6] Puiroux, N., Prat, M., and Quintard, M., "Non-equilibrium theories for macroscale heat transfer: ablative composite layer system," *International Journal of Thermal Sciences*, Vol. 43, No. 6, 2004, pp. 541–554.

[7] Lachaud, J. and Mansour, N. N., "Porous material analysis toolbox based on OpenFoam and applications," *Journal of Thermophysics and Heat Transfer*, Vol. 28, No. 2, 2014, pp. 191–202, doi: 10.2514/1.T4262.

[8] Lachaud, J., van Eekelen, T., Scoggins, J. B., Magin, T. E., and Mansour, N. N., "Detailed chemical equilibrium model for porous ablative materials," *International Journal of Heat and Mass Transfer*, Vol. 90, 2015, pp. 1034–1045, doi:10.1016/j.ijheatmasstransfer.2015.05.106.

[9] Anderson, J. D., *Hypersonic and high temperature gas dynamics*, Mac Graw-Hill, New-York, 1989.

[10] Duffa, G., *Ablative Thermal Protection Systems Modeling*, AIAA, 2013, doi: 10.2514/4.101717.

[11] Savage, G., *Carbon/Carbon composites*, Chapman & Hall, London, 1993.

[12] Suzuki, T., Fujita, K., Yamada, T., Inatani, Y., and Ishii, N., "Postflight Thermal Protection System Analysis of Hayabusa Reentry Capsule," *Journal of Spacecraft and Rockets*, Vol. 51, No. 1, 2014, pp. 96–105, doi: 10.2514/1.A32549.

[13] Tran, H. K., Johnson, C. E., Rasky, D. J., Hui, F. C. L., Hsu, M.-T., Chen, T., Chen, Y. K., Paragas, D., and Kobayashi, L., "Phenolic Impregnated Carbon Ablators (PICA) as Thermal Protection Systems for Discovery Missions," Tech. Rep. 110440, NASA Technical Memorandum, 1997.

[14] Stackpoole, M., Sepka, S., Cozmuta, I., and Kontinos, D., "Post-Flight Evaluation of Stardust Sample Return Capsule Forebody Heatshield Material," AIAA paper 2008-1202, 2008, 12 p.

[15] Wright, M. J., Beck, R., Edquist, K., Driver, D., Sepka, S., Slimko, E., Willcockson, W., DeCaro, T., and Hwang, H., "Sizing and Margins Assessment of the Mars Science Laboratory Aeroshell Thermal Protection System," AIAA paper 2009-4231, 2009.

[16] Edquist, K. T., Hollis, B. R., Johnston, C. O., Bose, D., White, T. R., and Mahzari, M., "Mars Science Laboratory Heat Shield Aerothermodynamics: Design and Reconstruction," *Journal of Spacecraft and Rockets*, Vol. 51, No. 4, 2014, pp. 1106–1124, doi: 10.2514/1.A32749.

[17] Ritter, H., Portela, P., Keller, K., Bouilly, J. M., and Burnage, S., "Development of a European ablative material for heatshields of sample return missions," 6th European Workshop on TPS and Hot structures, Stuttgart, Germany, 1-3 April 2009.

[18] Wong, H.-W., Peck, J., Bonomi, R., Assif, J., Reinisch, G., Lachaud, J., and Mansour, N. N., "Quantitative determination of species production from the pyrolysis of a phenol-formaldehyde resin," *Polymer Degradation and Stability*, , No. 112, 2015, pp. 122–131, doi:10.1016/j.polymdegradstab.2014.12.020.

[19] Lachaud, J., Magin, T., Cozmuta, I., and Mansour, N. N., "A short review of ablative material response models and simulation tools," *Proceedings of the 7th Aerothermodynamics Symposium, 9-12 May 2011, Brugge, Belgium. ESA SP-692*, edited by L. Ouwehand, ESA Publications Division, ESTEC, Noordwijk, The Netherlands, 2011, ISBN : 978-92-9221-256-8.

[20] Moyer, C. B. and Rindal, R. A., "An Analysis of the coupled chemically reacting boundary layer and charring ablator: Part II," *NASA CR*, Vol. 1061, 1968, 168 p.

[21] Covington., M. A., Heinemann, J. M., Chen, Y.-K., Terrazas-Salinas, I., Balboni, J. A., Olejniczak, J., and Martinez, E. R., "Performance of a Low Density Ablative Heat Shield Material," *Journal of Spacecrafts and Rockets*, Vol. 45, No. 4, 2008, pp. 856–864.

[22] Milos, F. and Chen, Y.-K., "Ablation and Thermal Response Property Model Validation for Phenolic Impregnated Carbon Ablator," *Journal of Spacecrafts and Rockets*, Vol. 47, No. 5, September-October 2010, pp. 786–805.

[23] Lachaud, J., Martin, A., Cozmuta, I., and Laub, B., "Ablation workshop test case - Version 1.1 - Feb. 2, 2011," Prepared for the 4th Ablation Workshop (1-3 March 2011, Albuquerque, New Mexico).

[24] Blanquart, G., Pepiot-Desjardins, P., and Pitsch, H., "Chemical mechanism for high temperature combustion engine relevent fuels with emphasis on soot precursors," *Combust. Flame*, Vol. 156, No. 3, 2009, pp. 588–607.

[25] Wright, M. J., Hughes, M., Calomino, A., and Barnhardt, M. B., "An overview of technology investments in the NASA entry systems modeling project," 2015, AIAA 2015-1892. Doi: 10.2514/6.2015-1892.

[26] on Climate Change, I. P., *Renewable Energy Sources and Climate Change Mitigation*, Cambridge University Press, 2011.

[27] Blasi, C. D., "Modeling chemical and physical processes of wood and biomass pyrolysis," *Progress in Energy and Combustion Science*, Vol. 34, 2008, pp. 47–90, doi:10.1016/j.pecs.2006.12.001.

[28] Pozzobon, V., Salvador, S., Bziana, J. J., El-Hafi, M., Maoult, Y. L., and Flamant, G., "Radiative pyrolysis of wet wood under intermediate heat flux: Experiments and modelling," *Fuel Processing Technology*, Vol. 128, 2014, pp. 319–330.

[29] Rubin, E. M., "Genomics of cellulosic biofuels," *Nature*, Vol. 454, No. 7206, 2008, pp. 841–845.

[30] Moran-Mirabal, J. M., "Chapter 1 - Advanced-Microscopy Techniques for the Characterization of Cellulose Structure and Cellulose-Cellulase Interactions," *Cellulose - Fundamental Aspects.*, edited by T. van de Ven and L. Godbout, Intechopen, 2013.

[31] Park, W. C., Atreya, A., and Baum, H. R., "Experimental and theoretical investigation of heat and mass transfer processes during wood pyrolysis," *Combustion and Flame*, Vol. 157, 2010, pp. 481–494.

[32] Couhert, C., Commandre, J.-M., and Salvador, S., "Is it possible to predict gas yields of any biomass after rapid pyrolysis at high temperature from its composition in cellulose, hemicellulose and lignin?" *Fuel 88 (2009) 408417*, Vol. 88, 2009, pp. 408–417.

[33] Mason, E. A. and Malinauskas, A. P., *Gas transport in porous media: the dusty-gas model*, Chemical engineering monographs, Elsevier, Amsterdam, 1983.

[34] Scoggins, J. B. and Magin, T. E., *Mutation++ user manual*, von Karman Institute for Fluid Dynamics, Rhode Saint Genese, Belgium, 2015, 1st edition.

[35] Scoggins, J. B. and Magin, T. E., "Development of Mutation++: Multicomponent Thermodynamic And Transport property library for Ionized plasmas written in C++," AIAA paper 2014-2966, 2014. doi: 10.2514/6.2014-2966.

APPENDIX : MULTICOMPONENT DIFFUSION WITH STRONG TEMPERATURE AND PRESSURE GRADIENTS

The problem studied involves strong gradients of species concentration, temperature, and pressure. Multicomponent diffusion is potentially an important contributor to mass transport. We recently derived a very convenient method that uses driving forces to estimate the bulk diffusion fluxes of mass $\mathcal{F}_k$ and energy $\mathcal{Q}_k$. The idea is to use the rigorous Maxwell model, while simplifying its integration in the conservation equations. A perspective is to apply an approach similar to the Dusty Gas Model [33] to directly obtain effective driving forces. As a first approximation in the continuum regime (small Knudsen number), we suggest to use a simple correction, inspired from the binary mixtures theory [2], to account for the porosity ϵ_g and the tortuosity η of the porous medium. It reads

$$\mathcal{F}^*{}_k = \frac{\epsilon_g}{\eta}\mathcal{F}_k \tag{19}$$

$$\mathcal{Q}*_k = \frac{\epsilon_g}{\eta}\mathcal{Q}_k \tag{20}$$

The bulk diffusion fluxes are given by [4, 34]

$$\mathcal{F}_k = \mathcal{F}_k^p \partial_x p + \mathcal{F}_k^T \partial_x T + \sum_{j\in N_g} \mathcal{F}_k^{\mu_j} \partial_x \mu_j \tag{21}$$

$$\sum_{k\in N_g} (\mathcal{Q}_k) = \mathcal{F}_h^p \partial_x p + \mathcal{F}_h^T \partial_x T + \sum_{j\in N_g} \mathcal{F}_h^{\mu_j} \partial_x \mu_j \tag{22}$$

where the μ_j are respectively the element mole fractions z_j in chemical equilibrium and the species mole fractions x_j in chemical non-equilibrium.

In chemical equilibrium the driving forces are given by [34]

$$\begin{aligned}
\mathcal{F}_k^p &= -\textstyle\sum_{i\in S} \rho_i \frac{M_k}{M_i} \nu_i^k \sum_{j\in S} D_{ij} \left(\frac{\partial x_j}{\partial p} + \frac{x_j - y_j}{p} \right) \\
\mathcal{F}_k^T &= -\textstyle\sum_{i\in S} \rho_i \frac{M_k}{M_i} \nu_i^k \sum_{j\in S} D_{ij} \left(\frac{\partial x_j}{\partial T} + \frac{k_{T_j}}{T} \right) \\
\mathcal{F}_k^{z_l} &= -\textstyle\sum_{i\in S} \rho_i \frac{M_k}{M_i} \nu_i^k \sum_{j\in S} D_{ij} \left(\frac{\partial x_j}{\partial z_l} \right) \\
\mathcal{F}_h^p &= -\textstyle\sum_{i\in S} \rho_i h_i \sum_{j\in S} D_{ij} \left(\frac{\partial x_j}{\partial p} + \frac{x_j - y_j}{p} \right) \\
\mathcal{F}_h^T &= -\textstyle\sum_{i\in S} \rho_i h_i \sum_{j\in S} D_{ij} \left(\frac{\partial x_j}{\partial T} + \frac{k_{T_j}}{T} \right) \\
\mathcal{F}_h^{z_l} &= -\textstyle\sum_{i\in S} \rho_i h_i \sum_{j\in S} D_{ij} \left(\frac{\partial x_j}{\partial z_l} \right)
\end{aligned} \tag{23}$$

In chemical non-equilibrium the driving forces are given by [34]

$$\begin{aligned}
\mathcal{F}_k^p &= -\rho_i \textstyle\sum_{j\in S} D_{ij} \frac{x_j - y_j}{p} \\
\mathcal{F}_k^T &= -\rho_i \textstyle\sum_{j\in S} D_{ij} \frac{k_{T_j}}{T} \\
\mathcal{F}_k^{z_l} &= -\rho_i D_{ij} \\
\mathcal{F}_h^p &= -\textstyle\sum_{i\in S} \rho_i h_i \sum_{j\in S} D_{ij} \frac{x_j - y_j}{p} \\
\mathcal{F}_h^T &= -\textstyle\sum_{i\in S} \rho_i h_i \sum_{j\in S} D_{ij} \frac{k_{T_j}}{T} \\
\mathcal{F}_h^{z_l} &= -\textstyle\sum_{i\in S} \rho_i h_i D_{ij}
\end{aligned} \tag{24}$$

The driving forces can be provided directly by the software Mutation++ [35], which is available open source.